PAPER

A numerical survey of parameters to reach ignition condition for axial compression of a large-sized field reversed configuration

To cite this article: Yilin LI *et al* 2024 *Plasma Sci. Technol.* **26** 055104

Plasma Sci. Technol. **26** (2024) 055104 (9pp) https://doi.org/10.1088/2058-6272/ad1c38

A numerical survey of parameters to reach ignition condition for axial compression of a large-sized field reversed configuration

Yilin LI (李宜霖), **Hui LIAO** (廖晖), **Haiyang ZHOU** (周海洋) **and Xuan SUN** (孙玄)*

Department of Plasma Physics and Fusion Engineering, School of Nuclear Science and Technology, University of Science and Technology of China, Hefei 230026, People's Republic of China

*E-mail of corresponding author: xsun@ustc.edu.cn

Received 11 September 2023, revised 5 January 2024
Accepted for publication 8 January 2024
Published 30 April 2024

Abstract

Field reversed configuration (FRC) is widely considered as an ideal target plasma for magneto-inertial fusion. However, its confinement and stability, both proportional to the radius, will deteriorate inevitably during radial compression. Hence, we propose a new fusion approach based on axial compression of a large-sized FRC. The axial compression can be made by plasma jets or plasmoids converging onto the axial ends of the FRC. The parameter space that can reach the ignition condition while preserving the FRC's overall quality is studied using a numerical model based on different FRC confinement scalings. It is found that ignition is possible for a large FRC that can be achieved with the current FRC formation techniques if compression ratio is greater than 50. A more realistic compression is to combine axial with moderate radial compression, which is also presented and calculated in this work.

Keywords: field reversed configuration, magnetized target fusion, axial compression

(Some figures may appear in colour only in the online journal)

1. Introduction

Magnetized target fusion (MTF), also known as the magneto-inertial fusion (MIF) [1–4], falls within a region of parameter space that is intermediate between the inertial confinement fusion (ICF) [5], having high density (10^{30}–10^{32} m^{-3}) and magnetic confinement fusion (MCF) [6] with a lower density (10^{18}–10^{20} m^{-3}). It features the compression of initially magnetized plasma into the condition of ignition using external drivers such as plasma jet [7, 8], solid liner [9, 10], Z-pinch [11], etc. The presence of magnetic fields in the initial target plasma is essential for the success of the MTF as the magnetic field could suppress the thermal transport and reduce particle and energy loss rate [12].

The target plasma could be a plasmoid that possesses a closed magnetic structure, such as the spheromak [13, 14] or FRC [15, 16], both of which belong to the compact toroid. FRC serves as an ideal target for compression due to its extremely high plasma β (ratio of the plasma pressure over the external magnetic field) and the zero magnetic field strength in the plasma core, which implies that less driver energy is wasted on the compression of the internal trapped flux during the adiabatic compression process. In addition, FRC is robust enough to withstand high-speed translations or severe distortion [17–19]. Moreover, it is suitable for isolation of the FRC from the confinement/burning chamber to the source region where any subsequent requirement such as current drive, heating, or compression is extremely difficult.

Several compression schemes based on FRC have been studied. For instance, a solid liner compression experiment [20] conducted by the Los Alamos National Laboratory (LANL) and Air Force Research Laboratory showed that an FRC could be compressed cylindrically by more than a factor of 10 [2], with a density that increased more than 100-fold, to $> 10^{24}$ m^{-3}. A magnetic compression experiment

* Author to whom any correspondence should be addressed.

performed on the FRX-C/LSM facility [21] proved that compression was very effective for heating the FRC plasma, and the heating result was consistent with the adiabatic scaling; a third example can be found in the FRC injection experiments (FIX), showing that the axial compression of FRC could result in improved confinement [22].

Many of the existing imploding methods are involved in the compression of an elongated FRC in the radial direction, and thus the plasma radius inevitably shrinks by a significant amount. It is well known that the particle confinement time [15, 16] of an FRC $\tau_N \propto R^2/\rho_i$ (where τ_N, R, and ρ_i are the particle confinement time, magnetic axis radius, and ion gyroradius in the external field) is approximately proportional to the square of the magnetic axis radius. Thus, the confinement time decreases during radial compression and a significant amount of particles and/or energy is lost before the stagnation phase. This observation was confirmed during the flux–magnetic compression experiments made on the FRX-C/LSM, where they found that particle and flux confinement times decreased roughly with the square of the plasma radius during compression [21]; when the FRC radius remained a constant or even increased slightly in the FIX compression experiment, the confinement time and the plasma lifetime improved considerably [22].

Apart from these experiments, a recent discovery has found that the collisional merging (CM) FRC [23–25] could yield a much more stable FRC; the representative was the C-2 series devices constructed by TAE Technologies, Inc [26]. In reference [27], the authors showed that the C-2W has achieved a record FRC lifetime. Though their approach was to obtain a steady-state or at least quasi-steady-state fusion plasma, it is intriguing to consider the formation of an FRC using the collisional-merging technique for the magnetic target fusion, because the enhanced confinement is friendlier to the FRC compression and will greatly reduce the speed required for compression, including the power of the driver.

In this paper, a new axial compression method is proposed which features a dominant axial compression of an FRC having a large volume. It is worth mentioning that an FRC axial compression experiment with high-speed translated θ-pinch plasma was conducted in the KMAX device [28] which shows that the FRC separatrix length was compressed to one third of the initial value while the radius expanded by ~57%, resulting in a ~16% increase in the electron temperature and ~26% in the density. This result is consistent with adiabatic compression.

In this study, we first consider a target FRC compressed in the axial direction, and then we propose axial compression with moderate radial compression. A numerical model based on two different FRC confinement time scalings is presented to explore both compression schemes. The parameter space of burning the FRC plasma in each confinement scaling is calculated, and the required initial parameters of the target FRC to achieve ignition are also calculated for different compression ratios, compression speeds, and FRC sizes. A high-density stable CM FRC is preferred in our model.

2. Proposed approach

The proposed scheme is illustrated in figure 1. First, a FRC target is formed either inside locally or translated to the burning chamber. Then, the high-density, high-speed plasmoids/jets are launched from the plasma injection chamber at an angle aiming toward the axial ends of the FRC. During this phase, the magnetic lines in the plasma injection chamber can be shaped by coils to facilitate the injection of the plasmoids/jets. These high-speed plasmoids/jets are expected to converge and press against each other, and then propagate in just the axial direction since all the perpendicular momentum would be canceled. Thus, an axial moving, high-temperature, high-density plasmoid piston (plasma liner) is formed. Finally, the continuous motion of this piston could compress the FRC target and heat the target to the fusion temperature.

For the driver to implode the FRC in the axial direction, compact toroids (CTs) or plasma liner are suggested instead of the traditional drivers. The CTs can be accelerated to hyper velocity [29, 30], while the plasma liner [31, 32] can be formed by hypersonic plasma jet merging, which has shown a high energy conversion efficiency from electrical energy into plasma kinetic energy [33]. Thus, one of the compressing scenarios could be several CTs compressing a target CT. Ideally, the compression speed has to be fast enough to prevent merging of the compressing CT with the target CT, although the merging may refuel the target CT plasma.

Compared to most of the existing MTF schemes, the axial compression of a large-volume FRC scheme has several advantages. A FRC with a larger radius has a longer lifetime, and hence it can minimize particle and energy loss during translation and merging. In addition, a long lifetime makes stability control and preheating of the FRC possible, which could yield a better target plasma, and it relaxes the requirement of the plasma piston speeds. The scheme also provides better confinement of the FRC particles and perhaps better stability during axial compression because the

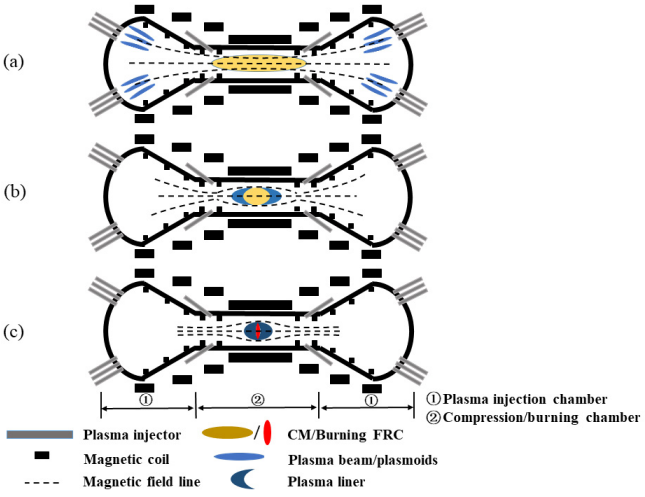

Figure 1. Axial compression of a large-sized FRC.

axial compression of the plasma piston aiming at the axial end of the FRC may impede the axial loss of the FRC particles as well as restrict the FRC motion to prevent tilt or elliptical deformation; then, the requirements for the compression speed and initial target parameters are expected to be relaxed. Further, a large target chamber volume can ensure the installation of internal magnetic coils for control of the magnetic geometry and translation of multiple plasma plasmoids/jets. Finally, the neutron wall loading should be considered in the design of the reactor, and hence a large volume is preferred.

It is worth noting that a large volume compression was performed in the ATC tokamak [34], and there is undergoing research at General Fusion to compress a 1 m spherical tokamak to 10 cm [35]. However, their approaches are significantly different from our proposal here, despite similarities in the energy recovery process and operation mode (pulsed reactor).

3. A numerical model

An axial compression numerical model (hereafter termed as the A-model) is established to study axial compression. One of the main objectives is to find a possible ignition condition. In our model, we consider an ideal driver with different initial velocities, and its kinetic energy is converted to the thermal energy of the target FRC. The separatrix radius R_s of FRC is a variable in the model and the elongation $E = Z/R_s$, where Z is half of the FRC length. In general, the FRC formed by the theta-pinch methods has $E \sim 3-30$ [16]. In our model, the initial elongation ratio $E = 8$ is specified. It is also assumed that the FRC has a homogeneous density and temperature, also with a uniform magnitude of internal magnetic field and closed magnetic field structure except in the vicinity of the O-point. Normally, the FRC expands radially during the axial compression process, the open magnetic line is squeezed, and an enhanced magnetic pressure is produced against the increased thermal pressure. Due to the well-conducting metal wall, the initial magnetic flux would be preserved, and the increased separatrix radius would be limited (no more than 1.5 times in our model) much smaller than the change of plasma length. Actually, the separatrix radius can be maintained by adding extra magnetic flux. Hence, to compare the axial compression with other compression results, we assume that the plasma radial size stays the same during axial compression in the A-model.

The temporal evolution of the target FRC is governed by the following five ordinary differential equations with time as the independent variable, and the equations of the A-model are as follows:

$$\frac{\mathrm{d}Z}{\mathrm{d}t} = v, \tag{1}$$

$$\frac{\mathrm{d}E_\mathrm{i}}{\mathrm{d}t} = P_\mathrm{wi} + P_\alpha - P_\mathrm{r} - \frac{E_\mathrm{i}}{\tau_\mathrm{E}}, \tag{2}$$

$$\frac{\mathrm{d}E_\mathrm{ks}}{\mathrm{d}t} = -P_\mathrm{wi}, \tag{3}$$

$$\frac{\mathrm{d}N_\mathrm{i}}{\mathrm{d}t} = -2R_\mathrm{DT} - \frac{N_\mathrm{i}}{\tau_\mathrm{N}}, \tag{4}$$

$$\frac{\mathrm{d}N_\mathrm{e}}{\mathrm{d}t} = -\frac{N_\mathrm{e}}{\tau_\mathrm{N}}. \tag{5}$$

These equations describe the basic physical processes during the compression process. For simplicity, the electrons and ions are assumed in the thermal equilibrium. Equation (1) shows the time change in the FRC length, where v is the compression velocity; equation (2) shows the change in the FRC thermal energy E_i, heated by the hydrodynamic work P_wi from the driver and by the deposition of the fusion alpha-particles P_α; the energy loss due to the radiative loss P_r (including the electron bremsstrahlung radiation P_bre and synchrotron radiation P_syn) is considered and the rest of the non-radiation loss channels, such as the thermal conductivity loss and convection loss, are included in the last term of equation (2), where τ_E represents the energy lifetimes, which can be obtained from different empirical scalings; equation (3) shows the expense of the driver kinetic energy $E_\mathrm{ks} = \frac{1}{2}M_s v^2$ (where M_s is the driver mass) on the compression, so the velocity v is advanced based on the consumption of the driver kinetic energy; equations (4) and (5) show the change in the number of particles, and the number of ions N_i in FRC decreases due to D–T reaction and particle loss, while the electron number N_e in FRC decreases only due to particle loss. Unlike many previous compression models where particle numbers are assumed to be conserved, the FRC particle losses based on different empirical scalings mentioned above are accounted for in the current A-model. The specific expression of τ_N will be mentioned in the following section. In our model, the plasmoid/jet particles are assumed to be unable to enter the closed magnetic field region, or inside FRC, on the compression time scale.

The five principal independent variables are Z, v, T, N_i, N_e. The rest of the quantities in the A-model can be derived from these variables with given initial conditions. The expressions for these quantities are given as

$$S_1 = \pi R_s^2, \tag{6a}$$

$$S_2 = 4\pi R_s Z, \tag{6b}$$

$$V = 2\pi R_s^2 Z, \tag{7}$$

$$n_\mathrm{i} = N_\mathrm{i}/V, \tag{8a}$$

$$n_\mathrm{e} = N_\mathrm{e}/V, \tag{8b}$$

$$P_\mathrm{wi} = 2S_1(n_\mathrm{i} + n_\mathrm{e})kTv, \tag{9}$$

$$E_{\rm i} = 1.5(n_{\rm i} + n_{\rm e})kTV, \tag{10}$$

$$\langle\beta\rangle_0 = 1 - R_{\rm s0}^2/2R_{\rm w0}^2, \tag{11}$$

$$B_{\rm in0} = \sqrt{2\mu_0(n_{\rm i0} + n_{\rm e0})kT_0(1/\langle\beta\rangle_0 - 1)}, \tag{12a}$$

$$E_{\rm b0} = B_{\rm in}^2 V_0 \big/ 2\mu_0, \tag{12b}$$

$$B_{\rm in} = \sqrt{2\mu_0 E_{\rm b0}/V}, \tag{13}$$

$$B_{\rm e}^2/2\mu_0 = B_{\rm in}^2/2\mu_0 + n_{\rm i}kT + n_{\rm e}kT, \tag{14}$$

where the target FRC is assumed to be cylindrical, and S_1 and S_2 are the areas of axial/radial surface of the FRC. $\langle\beta\rangle$ is the ratio of the averaged plasma pressure over the external magnetic field. It can be calculated using the so-called "average-β relation" (equation (11)), which is deduced from the axial force balance of a simple elongated FRC [36], though it may no longer be valid during the dynamic compression process. From equation (11), the volume averaged internal magnetic field $B_{\rm in}$ and the energy $E_{\rm b0}$ can be adaptively calculated by equation (12). There are no radial density or temperature profiles specified in our calculation, so the right-hand side of equation (14) is the volume averaged values. Because the FRC's thermal energy is about $\langle\beta\rangle/(1-\langle\beta\rangle)$ times larger than the internal magnetic energy [16], the pressure term dominates the internal magnetic energy term. Hence, the contribution to the evolution of $B_{\rm e}$ is mainly from the variation of pressure due to hydrodynamic work.

The DT reaction rate is

$$R_{\rm DT} = 0.25\langle\sigma v\rangle_{\rm DT} N_{\rm i}^2/V, \tag{15}$$

where $\langle\sigma v\rangle_{\rm DT}$ is the fusion cross-section, and for the Maxwellian velocity distribution plasma, it is just a function of the plasma temperature, given as

$$\langle\sigma v\rangle_{\rm DT} = C_1 \cdot \theta \sqrt{\frac{\xi}{1124656T^3}} {\rm e}^{-3\xi}, \tag{16}$$

where $\theta = T \Big/ \left[1 - \dfrac{T(C_2 + T(C_4 + TC_6))}{1 + T(C_3 + T(C_5 + TC_7))}\right]$, $\xi = (B_{\rm G}^2/(4\theta))^{1/3}$, and $B_{\rm G}$ is Gamov constant. The coefficient value can be found in the published paper [37]. The alpha heating power is

$$P_\alpha = f_\alpha \varepsilon_\alpha R_{\rm DT}, \tag{17}$$

where the energy fraction of the ε_α (3.5 MeV) alpha particles f_α in the FRC target is an approximate formula for the magnetized DT cylinders, which was provided by Basko *et al* in their published paper [38], and it also has been used by Li *et al* in their collision-merging FRC based solid-liner compression model [39].

$$P_{\rm bre} = 1.445 \times 10^{-40} g_{\rm ff} n_{\rm e} T_{\rm e}^{1/2} \sum n_{\rm i} Z_{\rm i}^2, \tag{18}$$

$$P_{\rm syn} = 6.2 \times 10^{-17} B^2 n_{\rm e} T_{\rm e}({\rm keV})[1 + T_{\rm e}({\rm keV})/204 + \ldots], \tag{19}$$

$$P_{\rm c} = S_1\kappa(T - T_{\rm b})/Z + S_2\kappa(T - T_{\rm b})/R_{\rm s}, \tag{20a}$$

$$\kappa = \kappa_{\perp{\rm e}} + \kappa_{\perp{\rm i}}. \tag{20b}$$

The total radiative loss of the radiation is $P_{\rm r} = P_{\rm bre} + P_{\rm syn}$ and the heat loss, $P_{\rm c}$, due to thermal conductivities, is shown in equation (20a). The expressions of perpendicular thermal conduction ($\kappa_{\perp{\rm e}}$ and $\kappa_{\perp{\rm i}}$) and the equations (18)–(20) can be found in [40]. It should be noted that the plasma plasmoid/jet temperature $T_{\rm b}$ in equation (20) is set to 100 eV, and the $g_{\rm ff}$ is set to 1.2. The thermal conductivity is classical in the equation. However, its contribution to the energy loss is lumped in an experimental loss rate $1/\tau_{\rm e}$ in equation (2), and hence there is no $P_{\rm c}$ term in equation (2). To check the effect of the classical thermal conduction loss, it is still calculated in the following section. This study and the numerical calculations employ the International System of Units (except equation (19)), and the initial values of all quantities are denoted by adding a subscript zero.

4. Adiabatic compression relationship and ignition region

First, we consider an ideal case in which there are no energy or particle losses to find the ignition region. In such case, or adiabatic compression, $PV^{5/3} = {\rm const}$, plasma pressure $P = 2nkT$, and, in this model, plasma volume V is reduced by the factor $C = V_0/V$ (where C is the volume convergence ratio). Hence, the plasma density n increases with C, the plasma temperature T increases with $C^{2/3}$, and the plasma thermal energy $E_{\rm i}$ increases with $C^{2/3}$. While assuming $E_{\rm b} = {\rm const}$, the internal magnetic field $B_{\rm in}$ increases with $C^{1/2}$.

4.1. Survey of burning FRC parameter regime

Before reporting the detailed compression process with specified FRC initial geometric parameters, a survey of the burning FRC parameter regime is conducted based on the above model. The FRC target ignition is reached if the alpha heating power surpasses the total power loss

$$P_\alpha - P_{\rm r} - \frac{E_{\rm i}}{\tau_{\rm E}} \geqslant 0. \tag{21}$$

Two FRC confinement time scalings are adopted in the calculation. One is the empirical law $\tau_{\rm N} = {\rm const}R^2/\rho_{\rm i}$ for the earliest FRC experiments $\tau_{\rm E} \approx 0.5\tau_{\rm N}$ and was first summarized by the FRX series devices at LANL [41]. In this case, it is termed as $\tau_{\rm N}^{\rm LANL}$, where $R = R_{\rm s}/\sqrt{2}$ is in the elongated FRCs and $\rho_{\rm i} = (m_{\rm i}kT_{\rm i})^{1/2}/eB_{\rm e}$, where $m_{\rm i}$ are 2.5 times the mass of the proton, e is the electron charge, and the const in

empirical law is 1×10^{-4} s m^{-1} [16]. The second one, $\tau_N^{C2}\sim10\tau_N^{LANL}$ with ten times better confinement, was adopted based on the C-2 series experiments in which a ten-fold improvement in the particle confinement was achieved [26]. It is worth of noting that the confinement can be further improved if the electron temperature can be increased, as indicated from their latest experimental report [42].

The ignition conditions for these two different confinement laws are shown in figures 2(a) and (b). Three radii are chosen to investigate the burning parameter regime of the FRC, namely, R_s = 0.03 m, the typical size of the solid-liner compression experiments; R_s = 0.3 m, the typical size of the C-2 FRC having better confinement; and an intermediate value of R_s = 0.1 m. Figure 2 clearly shows that the C-2 scaling possesses a wider parameter space for reaching ignition condition. For both scaling laws, the ignition threshold density decreases with the increase in the FRC size. This is because the confinement time increases quadratically with the increased radius and subsequently lowers the required lowest density. There are upper- and lower-temperature limits in our model. The ratios of P_α/P_{bre}, P_α/P_{syn}, P_{bre}/P_{syn} are shown in figure 2(c) with the red, blue, and purple lines respectively, and the red circle indicates the minimum ignition temperature or ideal ignition temperature, ~4.7 keV, when P_{syn} is negligible, while the blue circle indicates the maximum ignition temperature determined by P_{syn}, which becomes dominant at higher temperature. The parameter region without P_{syn} is also investigated and is presented in figures 2(a) and (b) along with the dotted lines, and shows a clear difference in the region of high temperature. It should be noted that these results are independent of the specific compression process.

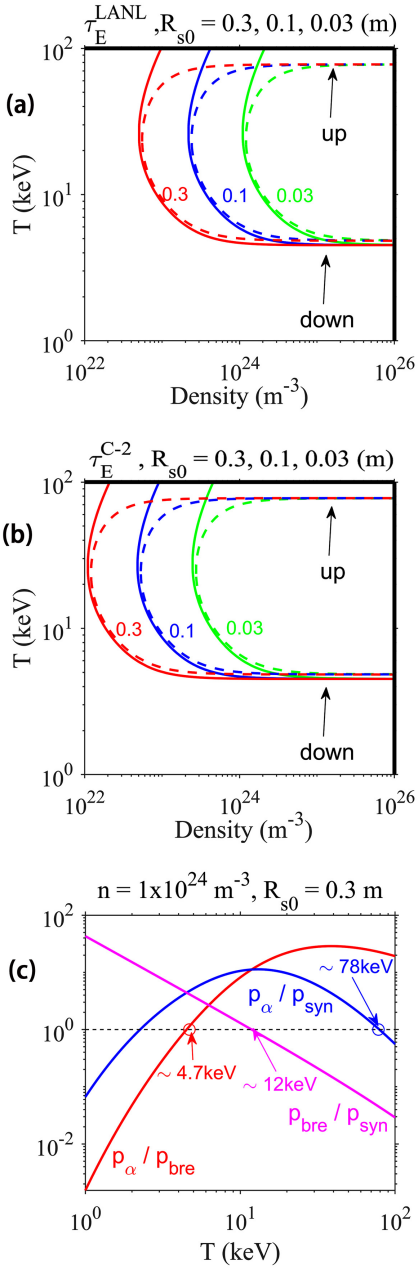

Figure 2. Parameter space of burning FRC with (a) LANL scaling, (b) C-2 scaling; the parameter region without P_{syn} is illustrated by dotted line. (c) Ratios of P_α/P_{bre}, P_α/P_{syn}, P_{bre}/P_{syn} at $n=1\times10^{24}$ m^{-3}, R_{s0} = 0.3 m.

4.2. Axial compression

It is essential to know if the axial compression alone can achieve the fusion goal based on the available experimental data and technique. In the computation, the initial kinetic energy of the driver is given as $E_{i0}C^{2/3}-E_{i0}$, which is the required driver energy in the adiabatic compression model. The program starts running from t = 0 and terminates when $V_0/V>C$ or the kinetic energy of the driver is exhausted (drive velocity below $0.01v_{s0}$).

An example with initial compression velocity of 50 km s^{-1} for both of the scalings introduced above is given in figure 3(a). The compression ratio C = 10, 50, 100, and different C correspond to different initial driver kinetic energies. The horizontal and vertical axes are the initial FRC temperature (100–1000 eV) and density ($1\times10^{20}-1\times10^{22}$ m^{-3}) respectively. Clearly a better confinement can reduce the requirements for initial target parameters, especially the minimum initial target density, as well as the requirements for the drive power.

With a fixed convergence ratio C (where C = 50), the influence of the initial compression velocity on the ignition condition is explored, and the results for different initial v_{s0} are shown in figure 3(b). In the case of LANL scaling, the lowest compression velocity v_{s0} = 1 km s^{-1}, which is the typical compression speed of solid liner. For C-2 scaling, the effect of increasing the compression speed is limited, and so does for the LANL scaling if the v_{s0} exceeds 10 km s^{-1}. It can be explained by comparing the compression time relative to the energy confinement time of the initial FRC in table 1, the compression time $\tau_{com}^{LANL}=\tau_{com}^{C-2}$ is only determined by the size of FRC, the speed of the driver, and the energy confinement time $\tau_{E0}^{C-2}=10\tau_{E0}^{LANL}$ calculated at $n_0=1\times10^{20}$ m^{-3}, R_{s0} = 0.3 m. For the compression speed, we choose τ_{com}^{C-2} that is less than or at least in the same order of magnitude of τ_{E0}^{C-2} at any compression speed. As for τ_{com}^{LANL},

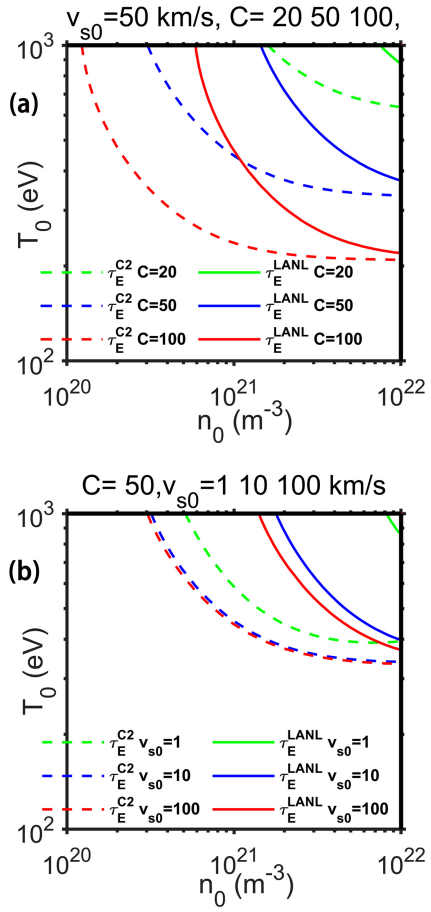

Figure 3. The ignition condition is explored with (a) fixed initial compression velocity (in this case $v_{s0} = 50$ km s^{-1}) along with different convergence ratio C, when C = 10, 50, 100 is investigated; (b) fixed convergence ratio C (here C = 50) and different initial compression velocities, when v_{s0} = 1, 10, 100 km s^{-1} is investigated.

Table 1. Comparison of typical compression time and energy confinement time at t = 0 is calculated at $R_{s0} = 0.3$ m, $n_0 = 1\times10^{20}$ m^{-3}.

v_{s0} (km s^{-1})	$\tau_{com}^{LANL} \approx \tau_{com}^{C\text{-}2}$ (ms)	τ_{E0}^{LANL} (ms)	$\tau_{E0}^{C\text{-}2}$ (ms)
1	~2.4	~0.14	~1.4
10	~0.25	~0.14	~1.4
100	~0.025	~0.14	~1.4

it was true only when the $v_{s0} > 10$ km s^{-1}. Thus, the results reveal that the compression needs to be completed in the confinement time range of the target plasma. Nevertheless, for a specific initial driver kinetic energy, a higher speed can lower the mass requirement of the driver.

Hence, one can optimize the compression velocity with the condition that the compression time is less than the characteristic lifetime of the FRC, $\tau_{com} < \tau_E$, and since $\tau_{com} \sim \sqrt{2}ER_0/\overline{v_s}$, $\tau_E = \text{const}R_0^2/\rho_{i0}$, one can have

$$\overline{v_s} > \text{const}E\big/R_0\sqrt{n}. \tag{22}$$

This equation shows that large volume FRC and higher initial density are more beneficial in reducing the required minimum compression speed. The numerical results are provided in figure 4, which are consistent with the above analysis. It indicates that the compression speed only needs to exceed 1 km s^{-1} when under a large FRC ($\geqslant 0.3$ m) with good confinement ($\tau_E^{C\text{-}2}$).

It is illuminating to investigate how the plasma parameters evolve during compression and an example is given below. Since this work is focused on compression of a large volume and long lifetime FRC plasma, collision-merging FRC parameters achieved in C-2 series experiments are much related to our model here; thus, C-2 scaling and parameters are referenced here. Initial FRC parameters were chosen as $n_0 = 5\times10^{20}$ m^{-3}, $T_i \sim T_e = 800$ eV, a total of 1.6 keV, which is 10 times the FRC density of the typical C-2W FRC parameter [43] with almost the same total temperature, the initial compression velocity v_{s0} is set to 50 km s^{-1}, and the convergence ratio C is set to 50. The evolution of all the parameters is presented in figure 5, which shows that the whole compression process lasts for about 0.05 ms. The temperature and density of the plasma increase to the expected values, and there is a slight deviation from the adiabatic relationship due to this loss. To maintain the radial dimension of the FRC and the radial pressure balance, the external magnetic field needs to be enhanced by increasing the current of the coils. The final external magnetic field is above 10 T, which is shown in figure 5(a), and the various heat/power losses can be seen in figure 5(c). The classic

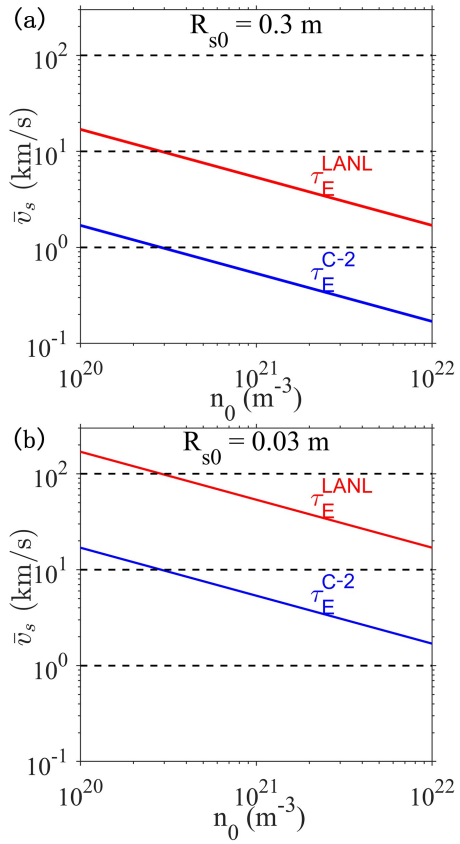

Figure 4. Calculated average compression speed $\overline{v_s}$ of equation (22) at (a) $R_{s0} = 0.3$ m, (b) $R_{s0} = 0.03$ m.

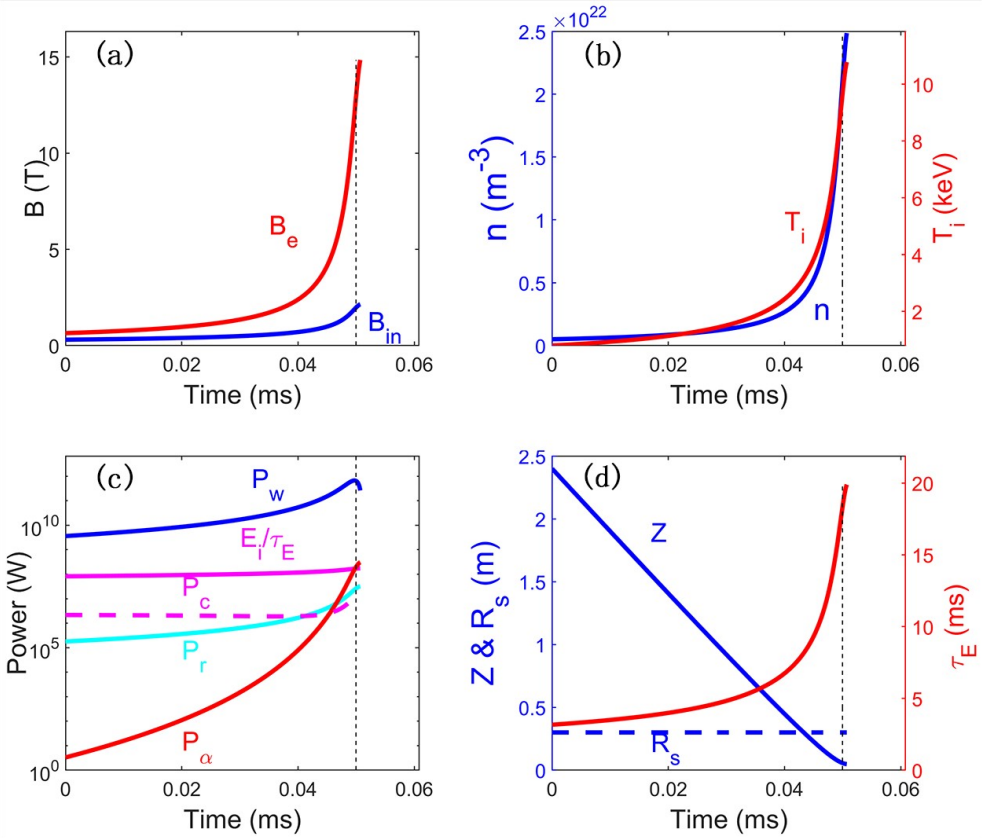

Figure 5. Time history of the FRC parameters. (a) Magnetic field, (b) target density and temperature, (c) heating/loss power, (d) FRC size and energy confinement time during the axial compression of an FRC (A-model) with $R_{s0} = 0.3$ m at C-2 scaling $n_0 = 5\times10^{20}$ m^{-3}, $T_i \sim T_e = 800$ eV, $v_{s0} = 50$ km s^{-1}, and $C = 50$. The black dotted line shows the ignition reached.

thermal conduction loss rate P_c, also shown in figure 5(c), is much lower than the energy loss calculated by the scaling laws. The evolution of the compression velocity is presented in figure 6. The ignition reached toward the end of compression is indicated by a black dotted line where the alpha heating power was beyond the total loss rate.

4.3. Axial compression with radial compression

Axial compression of $C = 50$ could yield an extreme oblate FRC ($E = 0.16$). To the authors' knowledge, no such FRC has been formed, which makes it an unknown area for the FRC study, and it is hard to predict how stable such FRC is. Also, it is unknown if such large-scale axial compressions could be achieved experimentally or not, though radial compression of greater than 10 times has been achieved before. The purpose of axial compressions is to minimize the particle/energy loss by maintaining the radial size of the FRC during compression, which is based on the current FRC confinement scaling. At the same time, the total volume compression ratio should not be too small. Thus, one can perceive that the compression can be performed simultaneously from the axial and radial directions, as long as the radial compression of the FRC is within reasonable limits.

Radial compression can be obtained through plasmoids, liquid wall compression, or just by energizing fast coils to increase the magnetic flux between the wall and the target

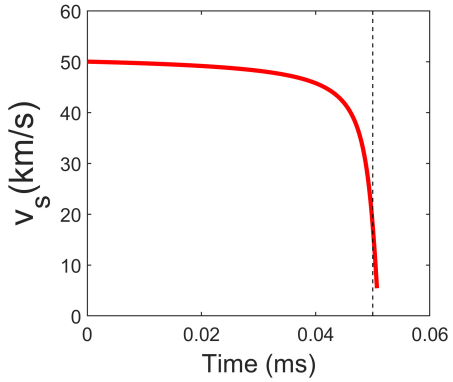

Figure 6. Time history of the compression velocity with initial velocity of 50 km s^{-1}. The black dotted line shows the ignition reached.

FRC. To investigate hybrid compression that consists of large-scale axial compression plus small-scale radial compression, the A-model has been modified to include radial compression equation (23), where α is an adjustable constant, and add radial compression work in equation (9), which is shown in equation (24); we termed this model the AR-model. To reach the ignition condition with a reasonable initial condition and compression ratio as well as confinement quality, we slightly adjust the initial density $n_0 = 7\times10^{20}$ m^{-3} and volume compression ratio $C = 60$, while temperature $T_i \sim T_e = 800$ eV and compression speed

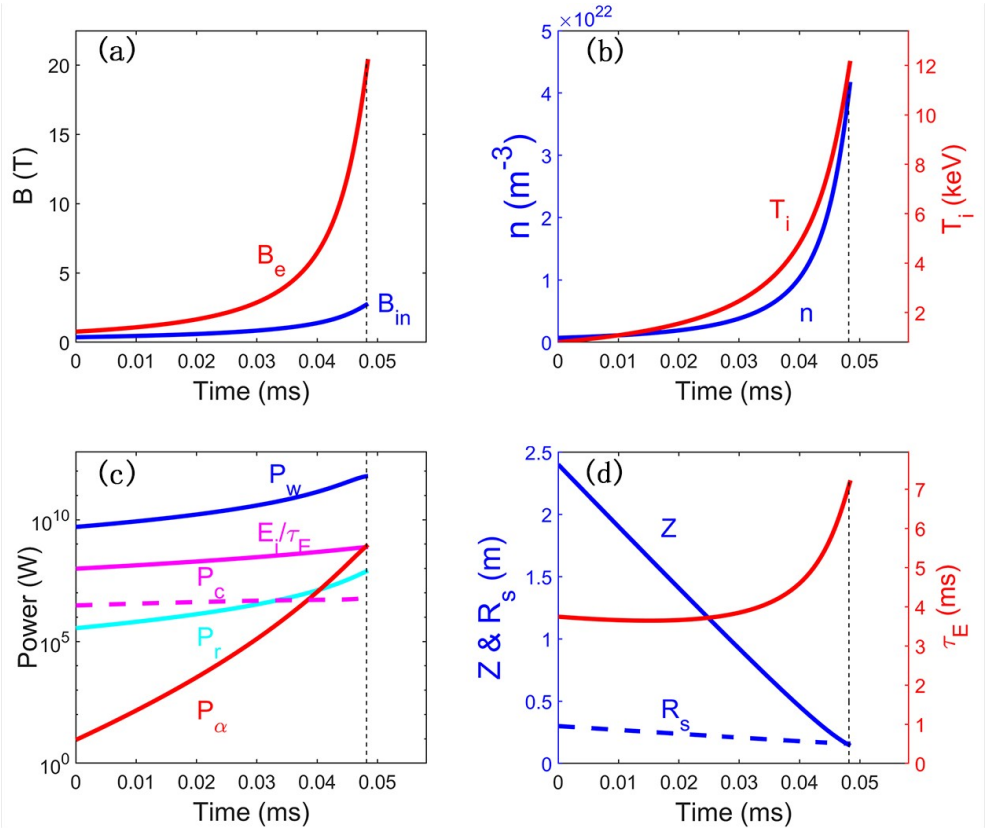

Figure 7. Time history of FRC parameters. (a) Magnetic field, (b) target density and temperature, (c) heating/loss power, (d) FRC size and time of energy confinement during axial compression of an FRC (AR-model) with $R_{s0} = 0.3$ m at C-2 scaling $n_0 = 7\times10^{20}$ m^{-3}, $T_i \sim T_e = 800$ eV, $v_{s0} = 50$ km s^{-1}, $C_z = Z_0/Z \sim 17$ and $C_r = R_0/R \sim 1.9$, and $C = 60$. The black dotted line shows that the ignition is reached.

$v_{s0} = 50$ km s^{-1} remain unchanged. Figure 7 shows the evolution of each target parameter for axial compression ratio $C_z = Z_0/Z \sim 17$ and radial compression ratio $C_r = R_0/R \sim 1.9$, which is similar to the case shown in figure 5, except τ_E (decreased in this case) and the final FRC $E \sim 1$, see figure 7 (d).

$$\frac{\mathrm{d}R_s}{\mathrm{d}t} = v_r,\ v_r = \alpha v, \tag{23}$$

$$P_{wi} = 2S_1(n_i + n_e)kTv + S_2(n_i + n_e)kTv_r. \tag{24}$$

5. Instability

The stability of the target FRC is critical to the success of the compression. Out of the three global principal instabilities of the FRC, tilting is the most dangerous and destructive [16]. Past experiments have shown that FRC can be stable, and the plasma can be well confined as long as the plasma remains within a kinetic regime. Stability and transport are both observed to have rapidly deteriorated when the kinetic condition exceeds $S^*/E > 5$ [44]. Here, $S^* = R_s/(c/\omega_{pi})$ is the radial size parameter, where c/ω_{pi} is the ion skin depth and $\omega_{pi} = e^2n/\varepsilon_0 m_i$ is the frequency of the ion plasma. For a fixed target FRC $E = 8$, the stability criterion versus density

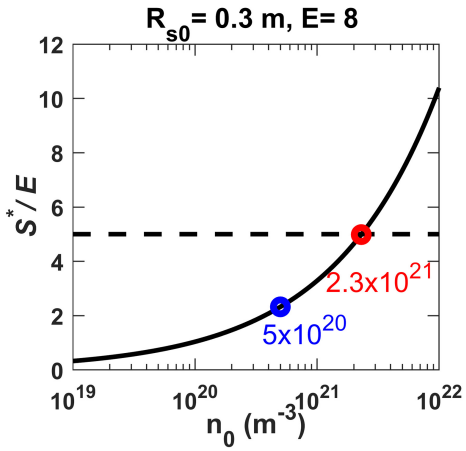

Figure 8. Stability criterion S^*/E versus n_0.

graph is plotted in figure 8. The cases chosen are shown in figures 5 and 7, where the initial density $n_0 = 5\times10^{20}$ m^{-3} (blue circle) is stable. It is also shown that the initial CM-FRC density should not be higher than $n_0 = 2.3\times10^{21}$ m^{-3} (red circle) during the current geometry model settings to ensure that the initial FRC is stable.

When performed with dominant axial compression, the density increased with a reduced axial length, and the FRC would be unstable if the above criterion is still applicable. However, this criterion is usually applicable to elongated-

steady FRC, and whether it works for dynamic FRC (translated FRC and FRC in compression) remains to be studied. More importantly, in our model, the FRC is surrounded by high density plasma liner, i.e., the axial boundary condition is different. The high-density plasma liner, with a much larger mass on either side of the FRC, forms an essentially high temperature "plasma conducting wall" which limits the plasma movement. Thus, the FRC may not increase the tilt instability due to the confinement of the "plasma wall" formed by the plasmoids/jets. However, it remains to be tested.

6. Summary

In summary, a novel scheme to compress a CM FRC is proposed. This proposal's two distinct features are a large volume target plasma for a long plasma lifetime and axial compression with moderate radial compression to preserve the confinement during compression. The driver is made of a plasma piston, which could be formed by CTs or plasma jets as long as it can deliver sufficient kinetic energy. In contrast with magnetic compression, most of our driver energy can be coupled to the plasma energy instead of increasing the internal magnetic energy during the adiabatic compression process. The merits of such compression are summarized below. First, particle confinement (energy confinement is closely correlated for FRC) can be maintained or at least kept from deterioration during the FRC compression. Further, a large volume plasma makes it easier to apply heating or control methods to yield a better initial plasma and is much more favorable for achieving fusion temperature. Second, the axial high-temperature high density plasma liner surrounding the target during the compression can play the role of a "plasma metal wall" which can improve the stability of the target FRC and axial particle confinement as well; moreover, it can prevent the target from swelling immediately after the compression peak.

The adiabatic relationship of the axial compression was derived, and an axial compression model (A-model) and axial plus radial compression model (AR-model) were also given to explore the FRC-based axial compression schemes. The minimum compression speed is related to the initial FRC radius and density, and as a result, it was found that the required compression speed of a large-volume FRC was relatively low. It is also shown that the "ignition condition" could be reached in a model at 50 times compression (v_{s0} = 50 km s^{-1}) with its initial parameters $n_0 \approx 5\times10^{20}$ m^{-3}, $T_i \sim T_e = 800$ eV, which is ten times higher than the current C-2 CM FRC density. A hybrid compression that consists of large-scale axial compression as well as small-scale radial compression was put forward; this operation scheme is expected to be much more feasible in the upcoming experimental demonstration. In the end, the stability of the initial CM FRC, as well as its stability during compression, has been discussed in brief. More studies need to be made in the future to demonstrate the feasibility of this concept.

Acknowledgments

This work was supported by National Natural Science Foundation of China (No. 12175226).

Data availability

The data that support the findings of this study are available within the article.

References

[1] Kirkpatrick R C, Lindemuth I R and Ward M S 1995 *Fusion Technol.* **27** 201
[2] Lindemuth I R and Siemon R E 2009 *Am. J. Phys.* **77** 407
[3] Wurden G A *et al* 2016 *J. Fusion Energy* **35** 69
[4] Lindemuth I R 2017 *Phys. Plasmas* **24** 055602
[5] Hurricane O A *et al* 2014 *Nature* **506** 343
[6] Ongena J *et al* 2016 *Nat. Phys.* **12** 398
[7] Zhang Y *et al* 2017 *Phys. Plasmas* **24** 110702
[8] Yates K C *et al* 2020 *Phys. Plasmas* **27** 062706
[9] Intrator T *et al* 2002 *Nucl. Fusion* **42** 211
[10] Martin M R *et al* 2012 *Phys. Plasmas* **19** 056310
[11] Gomez M R *et al* 2014 *Phys. Rev. Lett.* **113** 155003
[12] Lindemuth I R and Kirkpatrick R C 1983 *Nucl. Fusion* **23** 263
[13] Jarboe T R 1994 *Plasma Phys. Control. Fusion* **36** 945
[14] Jarboe T R 2005 *Phys. Plasmas* **12** 058103
[15] Tuszewski M 1988 *Nucl. Fusion* **28** 2033
[16] Steinhauer L C 2011 *Phys. Plasmas* **18** 070501
[17] Rej D J *et al* 1986 *Phys. Fluids* **29** 852
[18] Himura H *et al* 1995 *Phys. Plasmas* **2** 191
[19] Kobayashi D and Asai T 2021 *Phys. Plasmas* **28** 022101
[20] Degnan J H *et al* 2013 *Nucl. Fusion* **53** 093003
[21] Rej D J *et al* 1992 *Phys. Fluids B: Plasma Phys.* **4** 1909
[22] Okada S *et al* 1999 *Nucl. Fusion* **39** 2009
[23] Votroubek G *et al* 2008 *J. Fusion Energy* **27** 123
[24] Binderbauer M W *et al* 2010 *Phys. Rev. Lett.* **105** 045003
[25] Lin M N *et al* 2017 *Rev. Sci. Instrum.* **88** 093505
[26] Binderbauer M W *et al* 2015 *Phys. Plasmas* **22** 056110
[27] Roche T *et al* 2021 *Rev. Sci. Instrum.* **92** 033548
[28] Liao H *et al* 2022 *Plasma Phys. Control. Fusion* **64** 105015
[29] Hammer J H *et al* 1988 *Phys. Rev. Lett.* **61** 2843
[30] Hammer J H *et al* 1991 *Phys. Fluids B: Plasma Phys.* **3** 2236
[31] Hsu S C and Langendorf S J 2019 *J. Fusion Energy* **38** 182
[32] Thio Y C F *et al* 2019 *Fusion Sci. Technol.* **75** 581
[33] Witherspoon F D *et al* 2009 *Rev. Sci. Instrum.* **80** 083506
[34] Bol K *et al* 1972 *Phys. Rev. Lett.* **29** 1495
[35] Laberge M 2019 *J. Fusion Energy* **38** 199
[36] Armstrong W T *et al* 1981 *Phys. Fluids* **24** 2068
[37] Bosch H S and Hale G M 1992 *Nucl. Fusion* **32** 611
[38] Basko M M, Kemp A J and Meyer-ter-Vehn J 2000 *Nucl. Fusion* **40** 59
[39] Li C G and Yang X J 2016 *Phys. Plasmas* **23** 102702
[40] Thio Y C *et al* 1999 Magnetized target fusion in a spheroidal geometry with standoff drivers In: *2nd International Symposium on Current Trend in International Fusion Research*
[41] Tuszewski M and Linford R K 1982 *Phys. Fluids* **25** 765
[42] Gota H *et al* 2017 *Nucl. Fusion* **57** 116021
[43] Gota H *et al* 2019 *Nucl. Fusion* **59** 112009
[44] Slough J, Votroubek G and Pihl C 2011 *Nucl. Fusion* **51** 053008